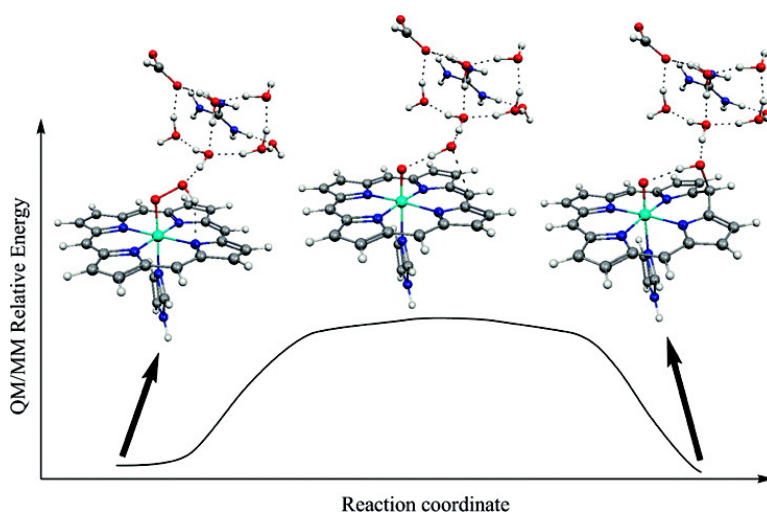**Article**

Quantum Mechanical/Molecular Mechanical Study of Mechanisms of Heme Degradation by the Enzyme Heme Oxygenase: The Strategic Function of the Water Cluster

Hui Chen, Yohann Moreau, Etienne Derat, and Sason Shaik

More About This Article

Additional resources and features associated with this article are available within the HTML version:

- Supporting Information
- Links to the 3 articles that cite this article, as of the time of this article download
- Access to high resolution figures
- Links to articles and content related to this article
- Copyright permission to reproduce figures and/or text from this article

View the Full Text HTML

Quantum Mechanical/Molecular Mechanical Study of Mechanisms of Heme Degradation by the Enzyme Heme Oxygenase: The Strategic Function of the Water Cluster

Hui Chen, Yohann Moreau, Etienne Derat,[#] and Sason Shaik*

Department of Organic Chemistry and the Lise Meitner-Minerva Center for Computational Quantum Chemistry, The Hebrew University of Jerusalem, Givat Ram Campus, 91904 Jerusalem, Israel
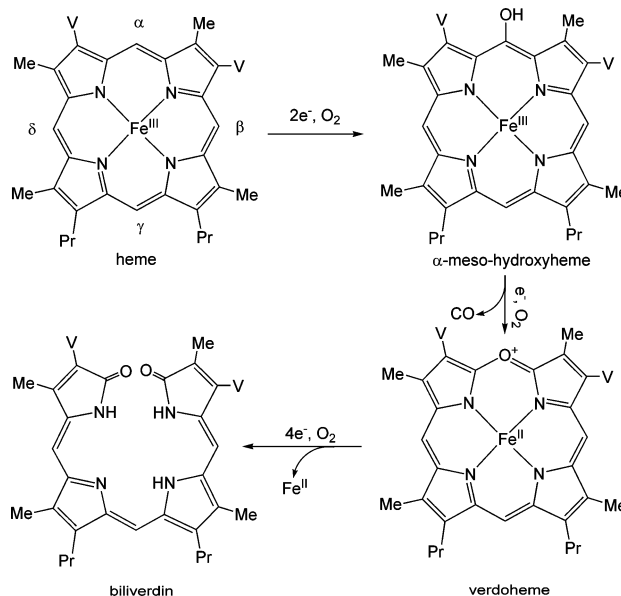
Received September 5, 2007; E-mail: sason@yfaat.ch.huji.ac.il

Abstract: Heme degradation by heme oxygenase (HO) enzymes is important in maintaining iron homeostasis and prevention of oxidative stress, etc. In response to mechanistic uncertainties, we performed quantum mechanical/molecular mechanical investigations of the heme hydroxylation by HO, in the native route and with the oxygen surrogate donor H_2O_2. It is demonstrated that H_2O_2 cannot be deprotonated to yield $Fe^{III}OOH$, and hence the surrogate reaction starts from the FeHOOH complex. The calculations show that, when starting from either $Fe^{III}OOH$ or $Fe^{III}HOOH$, the fully concerted mechanism involving O−O bond breakage and O−C$_{meso}$ bond formation is highly disfavored. The low-energy mechanism involves a nonsynchronous, effectively concerted pathway, in which the active species undergoes first O−O bond homolysis followed by a barrier-free (small with $Fe^{III}HOOH$) hydroxyl radical attack on the *meso* position of the porphyrin. During the reaction of $Fe^{III}HOOH$, formation of the Por$^{+•}Fe^{IV}$=O species, compound I, competes with heme hydroxylation, thereby reducing the efficiency of the surrogate route. All these conclusions are in accord with experimental findings (Chu, G. C.; Katakura, K.; Zhang, X.; Yoshida, T.; Ikeda-Saito, M. *J. Biol. Chem.* **1999**, *274*, 21319). The study highlights the role of the water cluster in the distal pocket in creating "function" for the enzyme; this cluster affects the O−O cleavage and the O−C$_{meso}$ formation*,* but more so it is responsible for the orientation of the hydroxyl radical and for the observed α-*meso* regioselectivity of hydroxylation (Ortiz de Montellano, P. R. *Acc. Chem. Res.* **1998**, *31*, 543). Differences/similarities with P450 and HRP are discussed.

1. Introduction

Heme oxygenase (HO) enzymes catalyze the degradation of heme to biliverdin, CO and free iron, in which the heme group functions as the prosthetic group as well as the substrate (see Scheme 1).[1−4] HO is abundant in nearly all classes of eukaryote and bacteria. For mammals, all three products of the HO-catalyzed heme degradation are physiologically important: released iron can maintain iron homeostasis, biliverdin plays a role in defense mechanism against oxidative stress, and CO can act as a neurotransmitter like NO. In cyanobacteria, algae, and plants, HO is involved in generating the chromophores for photosynthesis.[5] In some pathogenic bacteria, HO could play a key role in acquiring the iron ions from the host heme and in protecting the bacteria from the toxicity of heme.[6] The mech-

Scheme 1. Three Steps in the Degradation of Heme Catalyzed by HO; V = Vinyl, Me = Methyl, Pr = Propionate

anism of heme activation by HO is probed in this study using hybrid quantum mechanical/molecular mechanical (QM/MM)

[#] Current address: Laboratoire de Chimie Organique, Institut de Chimie Moléculaire, Université Pierre et Marie Curie-Paris 6, 4 place Jussieu B. 229, 75505 Paris, France.

(1) (a) Ortiz de Montellano, P. R. *Acc. Chem. Res.* **1998**, *31*, 543. (b) Colas, C.; Ortiz de Montellano, P. R. *Chem. Rev.* **2003**, *103*, 2305. (c) Ortiz de Montellano, P. R. *Curr. Opin. Chem. Biol.* **2000**, *4*, 221. (d) Ortiz de Montellano, P. R.; Wilks, A. *Adv. Inorg. Chem.* **2001**, *51*, 359.

(2) Sono, M.; Roach, M. P.; Coulter, E. D.; Dawson, J. H. *Chem. Rev.* **1996**, *96*, 2841.

(3) Yoshida, T.; Migita, C. T. *J. Inorg. Biochem.* **2000**, *82*, 33.

(4) Unno, M.; Matsui, T.; Ikeda-Saito, M. *Nat. Prod. Rep.* **2007**, *24*, 553.

(5) (a) Rhie, G.; Beale, S. I. *Arch. Biochem. Biophys.* **1995**, *320*, 182. (b) Willows, R. D.; Mayer, S. M.; Foulk, M. S.; DeLong, A.; Hanson, K.; Chory, J.; Beale, S. I. *Plant Mol. Biol.* **2000**, *43*, 113.

calculations of the processes within the native enzyme in the natural route and in the presence of surrogate oxidants (H_2O_2).

Several mammalian and bacterial HOs have been crystallized and characterized, among them are human HO-1,[7] rat HO-1,[8] and those from bacterium, like HmuO from *Corynebacterium diphtheriae*,[9] HemO from *Neisseria meningitides*,[10] PigA from *Pseudomonas aeruginosa*,[11] and Syn HO-1 and Syn HO-2 from cyanobacterium *Synechocystis*.[12] These HOs, coming from different sources, were found to have similar folds, in which heme is sandwiched between two helices, termed proximal and distal, and its edge is exposed to the enzyme surface. The proximal residue for heme in HO is histidine, which is common also to all the peroxidase family.[1a,2] The sequences of the distal residues, for mammalian HO-1 and HmuO, are highly conserved, but not so strictly in HemO and PigA.[4] HmuO exhibits 33% identical and 70% similarity with human HO-1.[13] Experimental results suggest that HmuO and mammalian HO share a similar mechanism for heme degradation.[14]

The overall catalytic reaction of HO requires three molecules of O_2 and seven electrons from NADPH-cytochrome P450 reductase or other electron donor.[15] Extensive experimental studies have established that the catalyzed reaction of HO proceeds through at least three steps as shown in Scheme 1.[16] Since the first step, in which the heme is converted to α-*meso*-hydroxyheme by hydroxylation of the α-*meso* position, is regioselective and governing the follow-up reactions, it has been studied more extensively than the subsequent two steps. The ferric hydroperoxide species, PorFe^{III}OOH, named hereafter, compound 0 (Cpd 0) was detected experimentally and proposed to be the active species during this first step of conversion.[17]

Several proposals have generally been suggested for the mechanism of this first heme activation step.[18] The first one involves electrophilic attack of OOH moiety of Cpd 0 on the α-*meso* carbon atom of the porphyrin ring. The second one involves homolytic cleavage of Cpd 0 to generate the OH radical followed by its attack on the α-*meso* carbon atom.[19] The third

one, which has been ruled out by the experimental results, is the nucleophilic attack of terminal oxygen atom of the ferric peroxide complex Fe^{III}-OO^{2-} on the α-*meso* carbon atom of the porphyrin ring.[20]

Experiments have shown that without adding any other reductant, reaction of HO with H_2O_2 can also produce α-*meso*-hydroxyheme complex, which is stable under anaerobic condition.[14a,18,21] This surrogate reaction with H_2O_2 was found to be less effective in HmuO than in mammalian HO but the reason is not yet clear. It was proposed that the surrogate reaction shares a same mechanism as the native route, with the normal O_2 plus NADPH-cytochrome P450 reductase-supported reaction, and it is thought that the active intermediate is also Cpd 0 (Fe^{III}OOH) formed after deprotonation of the H_2O_2.[14a] However, from the HO crystal structure, there are no appropriate basic side chains near the active site, which can facilitate this deprotonation process for iron coordinated H_2O_2 in HO. There is a robust cluster of eight crystal water molecules, which may act as a base, and this possibility is tested here.

Through deuterium kinetic solvent isotope effect and secondary carbon isotope effect measurements for human HO-1, Davydov et al. have argued that the rate-determining step from hydroperoxo-ferri-HO species to ferric-α-*meso*-hydroxyheme intermediate must involve a second proton delivery to FeOOH species from the solvent. In addition, classical interpretation for the observed secondary isotope effect led to a conclusion that O$-$C$_{\alpha-meso}$ bond formation must be involved in the rate-determining process of the heme hydroxylation.[22]

On the side of theory, two groups, ours[19] and Yoshizawa's,[23] have performed density functional studies with some model systems of the active site of HO and explored the possible mechanism of the first catalytic step of HO. The two groups found that the concerted heme degradation from Cpd 0, in which the O$-$O cleavage and O$-$C$_{\alpha-meso}$ bond formation occur simultaneously, has a very high barrier and is energetically prohibited. Two alternative mechanisms were suggested by the two groups: Thus, our group[19] proposed that the actual mechanism of action of HO involves homolysis of the O$-$O bond of Cpd 0, leading to a bound OH radical that attacks the α-*meso* position and generates the heme α-*meso*-hydroxylated intermediate. On the other hand, Yoshizawa et al.[23b] proposed that Cpd 0 undergoes initially heterolytic O$-$O bond cleavage

(6) (a) Zhu, W.; Hunt, D. J.; Richardson, A. R.; Stojiljkovic, I. *J. Bacteriol.* **2000**, *182*, 439. (b) Schmitt, M. P. *Infect. Immun.* **1997**, *65*, 4634.
(7) Schuller, D. J.; Wilks, A.; Ortiz de Montellano, P. R.; Poulos, T. L. *Nat. Struct. Biol.* **1999**, *6*, 860.
(8) Sugishima, M.; Omata, Y.; Kakuta, Y.; Sakamoto, H.; Noguchi, M.; Fukuyama, K. *FEBS Lett.* **2000**, *471*, 61.
(9) (a) Chu, G. C.; Park, S. Y.; Shiro, Y.; Yoshida, T.; Ikeda-Saito, M. *J. Struct. Biol.* **1999**, *126*, 171. (b) Unno, M.; Matsui, T.; Chu, G. C.; Couture, M.; Yoshida, T.; Rousseau, D. L.; Olson, J. S.; Ikeda-Saito, M. *J. Biol. Chem.* **2004**, *279*, 21055. (c) Hirotsu, S.; Chu, G. C.; Unno, M.; Lee, D. S.; Yoshida, T.; Park, S. Y.; Shiro, Y.; Ikeda-Saito, M. *J. Biol. Chem.* **2004**, *279*, 11937.
(10) (a) Zhu, W.; Wilks, A.; Stojiljkovic, I. *J. Bacteriol.* **2000**, *182*, 6783. (b) Schuller, D. J.; Zhu, W.; Stojiljkovic, I.; Wilks, A.; Poulos, T. L. *Biochemistry* **2001**, *40*, 11552.
(11) (a) Ratliff, M.; Zhu, W.; Deshmukh, R.; Wilks, A.; Stojiljkovic, I. *J. Bacteriol.* **2001**, *183*, 6394. (b) Friedman, J.; Lad, L.; Li, H.; Wilks, A.; Poulos, T. L. *Biochemistry* **2004**, *43*, 5239.
(12) (a) Sugishima, M.; Migita, C. T.; Zhang, X.; Yoshida, T.; Fukuyama, K. *Eur. J. Biochem.* **2004**, *271*, 4517. (b) Sugishima, M.; Hagiwara, Y.; Zhang, X.; Yoshida, T.; Migita, C. T.; Fukuyama, K. *Biochemistry* **2005**, *44*, 4257.
(13) Schmitt, M. P. *J. Bacteriol.* **1997**, *179*, 838.
(14) (a) Chu, G. C.; Katakura, K.; Zhang, X.; Yoshida, T.; Ikeda-Saito, M. *J. Biol. Chem.* **1999**, *274*, 21319. (b) Chu, G. C.; Tomita, T.; Sonnichsen, F. D.; Yoshida, T.; Ikeda-Saito, M. *J. Biol. Chem.* **1999**, *274*, 24490. (c) Wilks, A.; Moënne-Loccoz, P. *J. Biol. Chem.* **2000**, *275*, 11686. (d) Chu, G. C.; Katakura, K.; Tomita, T.; Zhang, X.; Sun, D.; Sato, M.; Sasahara, M.; Kayama, T.; Ikeda-Saito, M.; Yoshida, T. *J. Biol. Chem.* **2000**, *275*, 17494.
(15) (a) Tenhunen, R.; Marver, H. S.; Schmid, R. *J. Biol. Chem.* **1969**, *244*, 6388. (b) Tenhunen, R.; Marver, H. S.; Schmid, R. *Proc. Natl. Acad. Sci. U.S.A.* **1968**, *61*, 748. (c) Yoshida, T.; Noguchi, M.; Kikuchi, G. *J. Biol. Chem.* **1980**, *255*, 4418. (d) Schacter, B. A.; Nelson, E. B.; Marver, H. S.; Masters, B. S. S. *J. Biol. Chem.* **1972**, *247*, 3601.
(16) (a) Tenhunen, R.; Marver, H.; Pimstone, N. R.; Trager, W. F.; Cooper, D. Y.; Schmid, R. *Biochemistry* **1972**, *11*, 1716. (b) Docherty, J. C.; Schacter, B. A.; Firneisz, G. D.; Brown, S. B. *J. Biol. Chem.* **1984**, *259*, 13066.

(17) (a) Davydov, R. M.; Yoshida, T.; Ikeda-Saito, M.; Hoffman, B. R. *J. Am. Chem. Soc.* **1999**, *121*, 10656. (b) Davydov, R.; Kofman, V.; Fujii, H.; Yoshida, T.; Ikeda-Saito, M.; Hoffman, B. M. *J. Am. Chem. Soc.* **2002**, *124*, 1798. (c) Davydov, R.; Chemerisov, S.; Werst, D. E.; Rajh, T.; Matsui, T.; Ikeda-Saito, M.; Hoffman, B. M. *J. Am. Chem. Soc.* **2004**, *126*, 15960. (d) Garcia-Serres, R.; Davydov, R. M.; Matsui, T.; Ikeda-Saito, M.; Hoffman, B. M.; Huynh, B. H. *J. Am. Chem. Soc.* **2007**, *129*, 1402. (e) Denisov, I. G.; Ikeda-Saito, M.; Yoshida, T.; Sligar, S. G. *FEBS Lett.* **2002**, *532*, 203.
(18) Wilks, A.; Ortiz de Montellano, P. R. *J. Biol. Chem.* **1993**, *268*, 22357.
(19) (a) Sharma, P. K.; Kevorkiants, R.; de Visser, S. P.; Kumar, D.; Shaik, S. *Angew. Chem., Int. Ed.* **2004**, *43*, 1129. (b) Kumar, D.; de Visser, S. P.; Shaik, S. *J. Am. Chem. Soc.* **2005**, *127*, 8204.
(20) Wilks, A.; Torpey, J.; Ortiz de Montellano, P. R. *J. Biol. Chem.* **1994**, *269*, 29553.
(21) (a) Liu, Y.; Moënne-Loccoz, P.; Loehr, T. M.; Ortiz de Montellano, P. R. *J. Biol. Chem.* **1997**, *272*, 6909. (b) Matera, K. M.; Takahashi, S.; Fujii, H.; Zhou, H.; Ishikawa, K.; Yoshimura, T.; Rousseau, D. L.; Yoshida, T.; Ikeda-Saito, M. *J. Biol. Chem.* **1996**, *271*, 6618. (c) Ishikawa, K.; Takeuchi, N.; Takahashi, S.; Matera, K. M.; Sato, M.; Shibahara, S.; Rousseau, D. L.; Ikeda-Saito, M.; Yoshida, T. *J. Biol. Chem.* **1995**, *270*, 6345.
(22) Davydov, R.; Matsui, T.; Fujii, H.; Ikeda-Saito, M.; Hoffman, B. M. *J. Am. Chem. Soc.* **2003**, *125*, 16208.
(23) (a) Kamachi, T.; Shestakov, A. F.; Yoshizawa, K. *J. Am. Chem. Soc.* **2004**, *126*, 3672. (b) Kamachi, T.; Yoshizawa, K. *J. Am. Chem. Soc.* **2005**, *127*, 10686.

to generate the oxo ferryl porphyrin radical cation, $Por^{\bullet+}Fe^{IV}=O$, so-called compound I (Cpd I), and a water molecule. Subsequently, Cpd I abstracts a hydrogen atom from the so-formed H_2O, which thereby hydroxylates the α-*meso* position of porphyrin. However, recent experimental results have shown if Cpd I ($Por^{\bullet+}Fe^{IV}=O$) is generated in HO, it functions as a peroxidase, leading to the one-electron reduced form Cpd II ($PorFe^{IV}=O$) that returns to the resting ferric state slowly without converting to α-*meso*-hydroxyheme.[24] This result rules out the Cpd I−H_2O mechanism. In addition, a recent study by Montellano et al.[25] of radical addition to heme of horseradish peroxidase (HRP), mutated to exhibit HO-like reactivity (albeit with different regioselectivity) demonstrated that radicals but not electrophilic species react with *meso* carbons of heme in HRP, thus implying that the HO-catalyzed heme degradation occurs likely through controlled radical reaction rather than through electrophilic addition.[25]

Despite the many efforts to decipher the mechanism of HO action, it is apparent that there are still significant discrepancies between the mechanisms derived from the theoretical results and the one from the experimental results. Among the many unresolved aspects, an interesting and urgent one is to verify whether the previously proposed stepwise mechanism of *meso*-hydroxylation with a bound hydroxyl radical[19] is actually valid within the native HO enzyme. In this work we present a detailed QM/MM exploration of the mechanism of the first step of HO catalyzed heme degradation. Using the QM/MM methodology, we address several issues that cannot be safely considered with model QM model calculations. For example, we are interested to elucidate the effect of the protein environment on the reaction mechanism and the function of the hydrogen-bond network of the water cluster in the distal pocket of HO.[7,9c,26] In addition, we also explore the mechanism of the HO-catalyzed heme degradation proceeding via the surrogate reaction with H_2O_2. On the basis of these two mechanisms we shall propose possible connections between the surrogate reaction and the physiological one (O_2 plus NADPH-cytochrome P450 reductase) and unify the two mechanisms if possible. We shall also attempt to compare the native route of HO with that of cytochrome P450.[1,2] Why does P450 proceed from Cpd 0 ($PorFe^{III}OOH$) onward to Cpd I ($Por^{\bullet+}Fe^{IV}=O$), while HO stops a Cpd 0 and uses it to activate the heme?

2. Computational Details

2.1. QM/MM Methodology and Software. The QM/MM calculations have been done using the Chemshell[27] application combining

Turbomole[28] and DL-POLY.[29] The hybrid B3LYP functional[30] was used throughout this study for the QM part, while the CHARMM22 force field[31] was used for the MM part. The active species of the enzyme, which is described by QM method, can interact with rest of the enzyme by electrostatic, London, and van der Waals interactions. The electrostatic embedding scheme is used to account for the polarization effect of QM part by the protein environment. The dangling bond at the QM/MM boundary was saturated by a hydrogen-link atom and treated in the framework of the charge-shift method.[32] All reported energies in this work are electronic energies.

QM/MM geometry optimization was done with Turbomole/DL-POLY using a double-ζ basis set (LACVP)[33] for all the atoms except the two oxygen atoms coordinated to iron, for which we used a double-ζ basis set augmented with polarization and diffuse functions (6-31+G-(d)),[34] which gives a better description of the important O−O cleavage process. The energy was corrected by QM/MM single point calculations with a larger basis set labeled B2, which describes iron by the Wachters all-electron basis set,[35] augmented with diffuse d and f polarization functions, all electronegative atoms (O and N) by 6-31+G(d), while the C and H atoms by 6-31G(d,p).

Setup of the System. To prepare suitable initial structures for the QM/MM calculations, we started from the experimental X-ray structure of dioxygen-bound HO, HmuO (PDB code 1V8X),[9b] which is the only X-ray structure of heme oxygenase available where the O_2 unit is bonded to iron. There are three equivalent subunits, namely A, B, and C in the X-ray structure, and we chose one of them, the B-subunit, for our QM/MM calculations. We modified the oxy heme species ($PorFe^{III}OO^-$) of the X-ray structure by adding a hydrogen atom to the distal oxygen to build our QM model of Cpd 0 ($PorFe^{III}OOH$). We built a complete model of the solvated enzyme by adding the missing hydrogen atoms and a 16-Å-thick water solvent layer. The system was further prepared according to standard procedures (see Supporting Information (SI) document). The entire system consists of 15273 atoms, including 11292 atoms in the solvent. This system was then relaxed by performing pure force field minimizations and molecular dynamics (MD) with the CHARMM22 force field as implemented in the CHARMM program,[36] during which the coordinates of the heme, the proximal ligand His20 and the outer 8-Å-thick water solvent layer were kept fixed.

2.2. Charged Residues and Total Charge of the System. The total charge of the so-generated system was −11, corresponding to the following protonated state of the various residues: Aspartates (Asp) and Glutamates (Glu) were used as negatively charged (Asp31, Asp61, Asp74, Asp86, Asp88, Asp108, Asp118, Asp121, Asp136, Asp154, Asp174, Asp187, Asp199, Asp210, Glu11, Glu21, Glu24, Glu41, Glu47, Glu57, Glu70, Glu81, Glu95, Glu114, Glu115, Glu156, Glu164, Glu175, Glu178, Glu184, Glu188, Glu191, Glu196), and arginines (Arg) and lysines (Lys) were used as positively charged (Arg36, Arg44, Arg64, Arg79, Arg85, Arg97, Arg99, Arg112, Arg117, Arg132, Arg145, Arg149, Arg177, Arg190, Lys13, Lys22, Lys34, Lys89, Lys168, Lys170, Lys173, Lys179, Lys195, Lys213). From the pK_a calculation by PROPKA,[37] at pH = 7, the histidines (His20, His25,

(24) Matsui, T.; Kim, S. H.; Jin, H.; Hoffman, B. M.; Ikeda-Saito, M. *J. Am. Chem. Soc.* **2006**, *128*, 1090.
(25) Wojciechowski, G.; Ortiz de Montellano, P. R. *J. Am. Chem. Soc.* **2007**, *129*, 1663.
(26) (a) Matsui, T.; Furukawa, M.; Unno, M.; Tomita, T.; Ikeda-Saito, M. *J. Biol. Chem.* **2005**, *280*, 2981. (b) Lad, L.; Wang, J.; Li, H.; Friedman, J.; Bhaskar, B.; Ortiz de Montellano, P. R.; Poulos, T. L. *J. Mol. Biol.* **2003**, *330*, 527. (c) Li, Y.; Syvitski, R. T.; Chu, G. C.; Ikeda-Saito, M.; La Mar, G. N. *J. Biol. Chem.* **2003**, *278*, 6651. (d) Li, Y.; Syvitski, R. T.; Auclair, K.; Ortiz de Montellano, P. R.; La Mar, G. N. *J. Am. Chem. Soc.* **2003**, *125*, 13392. (e) La Mar, G. N.; Asokan, A.; Espiritu, B.; Yeh, D. C.; Auclair, K.; Ortiz de Montellano, P. R. *J. Biol. Chem.* **2001**, *276*, 15676. (f) Syvitski, R. T.; Li, Y.; Auclair, K.; Ortiz de Montellano, P. R.; La Mar, G. N. *J. Am. Chem. Soc.* **2002**, *124*, 14296. (g) Li, Y.; Syvitski, R. T.; Auclair, K.; Wilks, A.; Ortiz de Montellano, P. R.; La Mar, G. N. *J. Biol. Chem.* **2002**, *277*, 33018. (h) Lad, L.; Schuller, D. J.; Shimizu, H.; Friedman, J.; Li, H.; Ortiz de Montellano, P. R.; Poulos, T. L. *J. Biol. Chem.* **2003**, *278*, 7834. (i) Sugishima, M.; Sakamoto, H.; Higashimoto, Y.; Omata, Y.; Hayashi, S.; Noguchi, M.; Fukuyama, K. *J. Biol. Chem.* **2002**, *277*, 45086. (j) Rodriguez, J. C.; Zeng, Y. H.; Wilks, A.; Rivera, M. *J. Am. Chem. Soc.* **2007**, *129*, 11730.
(27) Sherwood, P.; et al. *J. Mol. Struct. (THEOCHEM)* **2003**, *632*, 1.
(28) Ahlrichs, R.; Bär, M.; Häser, M.; Horn, H.; Kölmel, C. *Chem. Phys. Lett.* **1989**, *162*, 165.
(29) Smith, W.; Forester, T. *J. Mol. Graph.* **1996**, *14*, 136.
(30) (a) Becke, A. D. *Phys. Rev. A* **1988**, *36*, 3098. (b) Lee, C.; Yang, W.; Parr, R. G. *Phys. Rev. B* **1988**, *37*, 785. (c) Becke, A. D. *J. Chem. Phys.* **1993**, *98*, 5648. (d) Becke, A. D. *J. Chem. Phys.* **1993**, *98*, 5648. (e) Becke, A. D. *J. Chem. Phys.* **1993**, *98*, 1372.
(31) MacKerell, A. D., Jr.; et al. *J. Phys. Chem. B* **1998**, *102*, 3586.
(32) Bakowies, D.; Thiel, W. *J. Phys. Chem.* **1996**, *100*, 10580.
(33) LACVP is constructed from the LANL2DZ basis sets: (a) Hay, J. P.; Wadt, W. R. *J. Chem. Phys.* **1985**, *82*, 299. (b) Friesner, R. A.; Murphy, R. B.; Beachy, M. D.; Ringlanda, M. N.; Pollard, W. T.; Dunietz, B. D.; Cao, Y. X. *J. Phys. Chem. A* **1999**, *103*, 1913.
(34) Hehre, W. J.; Ditchfield, R.; Pople, J. A. *J. Chem. Phys.* **1972**, *56*, 2257.
(35) Wachters, A. J. H. *J. Chem. Phys.* **1970**, *52*, 1033.
(36) Brooks, B. R.; Bruccoleri, R. E.; Olafson, B. D.; States, D. J.; Swaminathan, S.; Karplus, M. *J. Comput. Chem.* **1983**, *4*, 187.

Scheme 2. Schematic View of the QM Model System Used in the Calculations[a]
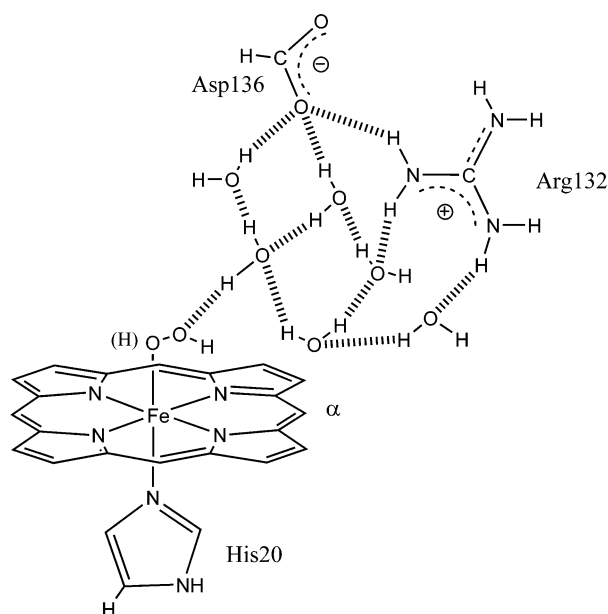
[a] The (H) is added to explore the H_2O_2 surrogate reaction.

His28, His29, His50, His62, His92, His105) were singly protonated and hence electronically neutral. Two more negative charges are located in the heme moiety.

2.3. The QM Region. According to many experimental investigations, the distal acid−base pair Arg132−Asp136 and several crystal waters that form a water cluster in the distal pocket are crucial for the proper catalysis function of HO. So our chosen QM part comprises iron-hydroperoxo porphyrin complex (without side chains of heme) with its proximal ligand His20 (modeled as imidazole), the distal residue Arg132 (modeled as $NH_2C^+(NH_2)_2$), Asp136 (modeled as $HCOO^-$), and six to seven crystal waters (the number depending on the snapshots, see the SI for more details), which form a water cluster through a hydrogen-bond network in the distal pocket. The QM region is shown in Scheme 2.

2.4. Optimized QM/MM Region. In addition to the active species and its Asp/water cluster group, 31 additional residues around heme were chosen to be relaxed in the QM/MM geometry optimization, and they are Lys13, Thr16, Ala19, His20 (including heme), Glu21, Ala23, Glu24, Met29, Leu33, Gln46, Tyr53, Tyr130, Val131, Arg132, Tyr133, Leu134, Gly135, Asp136, Leu137, Ser138, Gly139, Gly140, Gln141, Val142, Ile143, Ala144, Phe160, Tyr161, Arg177, Phe201, Phe208. Finally, some other crystal and solvent waters, which are hydrogen-bonded either with the carboxylate group of heme or to some charged residues of the QM/MM geometry optimization region, were included too (see SI for more details).

2.5. Snapshots. To assess the effect of different conformations of the enzyme, especially the different forms of water cluster in the distal pocket on the heme degradation process, except the 0 ps snapshot (close to the X-ray structure), we investigated two additional snapshots (after 116 and 287 ps of equilibration) from an MD trajectory obtained in the preparatory force field calculations. These two snapshots were selected because they have a different shape of water cluster in the distal pocket compared with that of the 0 ps snapshot.

3. Results

3.1. Molecular Dynamics Simulations. As mentioned above, to assess the effect of different conformations of the enzyme, and the different forms of the distal water cluster, on the heme
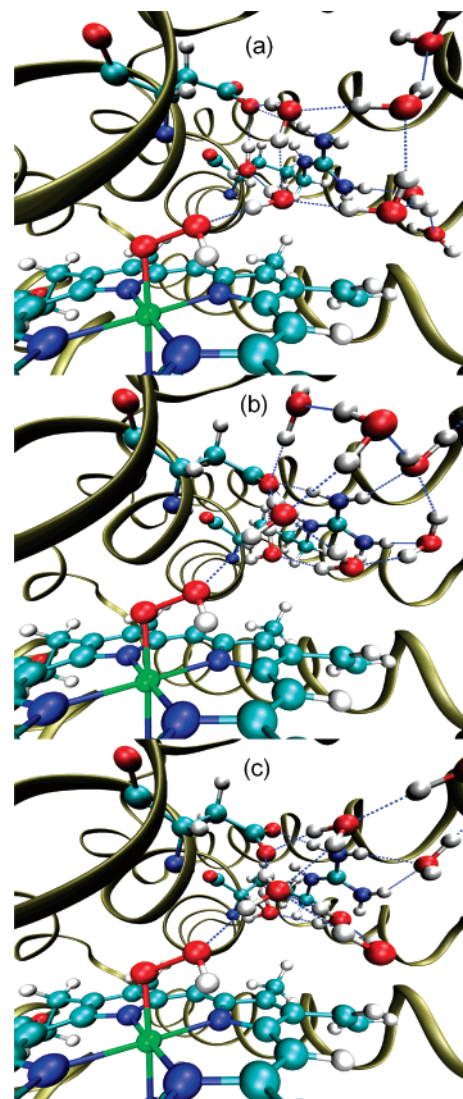
(37) Li, H.; Robertson, A. D.; Jensen, J. H. *Proteins* **2005**, *61*, 704.

Figure 1. Three snapshots of the MD trajectory at (a) 0, (b) 116, and (c) 287 ps. The point-of-view is looking forward from the *β-meso*-edge of the heme toward the *δ-meso*-edge of the heme. The heme, residues Arg132 and Asp136, and the crystal waters in the distal pocket are all shown explicitly.

degradation process, we performed CHARMM molecular dynamics simulations for 300 ps starting from the structure obtained after the setup procedure from X-ray structure and with fixed coordinates of the heme, His20 and the outer (8−16 Å) water solvent layer. Two snapshots, at 116 and 287 ps of the simulation separately, were picked up and were then subjected to pure force field energy minimizations, for subsequent QM/MM optimizations. Figure 1 shows the structure of the 116 and 287 ps snapshots as well as the 0 ps snapshot, all after pure force field energy minimizations. In 0, 116, and 287 ps snapshots, the shapes of the water clusters in the distal pocket are quite different. In the 0 ps snapshot, five water molecules and the oxygen atom of carboxyl group in Asp136 form two square clusters sharing one edge, while in the 116 ps snapshot, six water molecules and the oxygen atom of carboxyl group in Asp136 form two square clusters and one pentagonal cluster sharing one edge with each other. In the 287 ps snapshot, the hydrogen-bond network has evolved to form a water cluster with an irregular shape. Another difference of the water clusters between the 0 ps snapshot and the other two snapshots, at the

Table 1. QM(UB3LYP)/MM(CHARMM) Relative Energies (kcal/mol) for Three Spin States of Cpd 0, with Basis B1 and B2[a]

spin state	singly occupied orbitals	snapshot 0 ps		snapshot 116 ps		snapshot 287 ps	
		B1	B2	B1	B2	B1	B2
^2C_R	$\pi_{yz}*$	0.00	0.00	0.00	0.00	0.00	0.00
^4C_R	$\pi_{yz}*d_{xz}\sigma_{z^2}*$	12.27	10.84	10.57	9.02	12.65	11.16
^6C_R	$\sigma_{xy}*d_{x^2-y^2}\pi_{yz}*d_{xz}\sigma_{z^2}*$	13.82	11.10	11.19	8.45	12.59	9.95

[a] The left-hand superscript signifies the spin state of the species.

Scheme 3. Orbital Occupancies of Cpd 0 for the Doublet, Quartet, and Sextet States
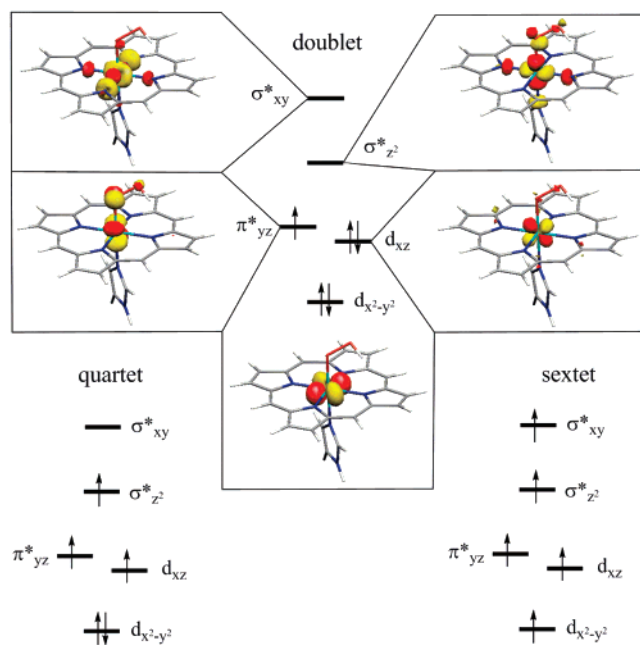
116 and 287 ps, is in the "link"-water molecule that forms a hydrogen bond with *the distal* O atom of FeOOH moiety, and thereby links FeOOH with the water cluster. In the 0 ps snapshot, this water connects with Asp136 through another bridging water molecule, while in the other two snapshots, it forms a hydrogen bond directly with Asp136. Despite these changes, no interactions develop between the water molecules and the *proximal oxygen* of FeOOH.

3.2. QM/MM Calculations. To probe the possible mechanism of the heme degradation, we explored mechanisms nascent from the Cpd 0 and Fe[III]HOOH species separately. Details of the numerical results are summarized in the Supporting Information. In the following, we focus on the key results.

3.2.1. Relative Spin State Energies and Geometries of Cpd 0 (PorFe[III]OOH). The calculated relative energies of various spin states of Cpd 0, labeled C_R are summarized in Table 1 for the three snapshots. One can see that in the protein environments of all three studied snapshots, the ground state of Cpd 0 is a doublet state with a singly occupied $\pi_{yz}*$ orbital, as shown in Scheme 3. For the 0, 116, and 287 ps snapshots, the quartet state, is 10.84, 9.02, and 11.16 kcal/mol higher than the doublet state at the QM/MM B2 level, respectively. In the three studied snapshots, the sextet state lies within an energy 0.6 kcal/mol of the quartet state. The electronic configuration of the quartet and the sextet states are, respectively, $d_{x^2-y^2}{}^2\pi_{yz}*{}^1d_{xz}{}^1\sigma_{z^2}*{}^1$ and $d_{x^2-y^2}{}^1\sigma_{xy}*{}^1\pi_{yz}*{}^1d_{xz}{}^1\sigma_{z^2}*{}^1$. It was proposed that the $d_{x^2-y^2}$ singly

occupied configuration is possibly involved in Cpd 0 of HO.[38] Our QM/MM results do not support this proposal: the QM/MM B2//B1 energy of the quartet state with the $d_{xz}{}^2\sigma_{xy}*{}^1d_{x^2-y^2}{}^1\pi_{yz}*{}^1$ configuration (for the 0 ps snapshot) is 5.7 kcal/mol higher than the original quartet Cpd 0 with $d_{x^2-y^2}{}^2\pi_{yz}*{}^1d_{xz}{}^1\sigma_{z^2}*{}^1$ configuration, whereas the doublet Cpd 0 with $\pi_{yz}*{}^2d_{xz}{}^2d_{x^2-y^2}{}^1$ configuration could not be located, and all our orbital swapping trials to get this state converged back to the doublet Cpd 0 with the $d_{x^2-y^2}{}^2d_{xz}{}^2\pi_{yz}*{}^1$ configuration. This result means that the doublet state with the $\pi_{yz}*{}^2d_{xz}{}^2d_{x^2-y^2}{}^1$ configuration is high in energy compared with the doublet Cpd 0 with $d_{x^2-y^2}{}^2d_{xz}{}^2\pi_{yz}*{}^1$ configuration. The latter result is consistent with the recent experimental results, which refuted the $d_{x^2-y^2}$ singly occupied configuration.[17d]

The key geometric parameters of the optimized structure for Cpd 0 in the three snapshots are collected in Table 2. One can see that for all the snapshots, the Fe$-$N$_{ImH}$ and Fe$-$O bond distances in the quartet and sextet states are about 0.2 Å longer than those in the doublet state, in line with the Fe$-$O and Fe$-$N$_{ImH}$ antibonding character of the $\sigma_{z^2}*$ orbital, which is singly occupied in the quartet and sextet states, but vacant in the doublet state. In the sextet states, the average Fe$-$N$_{por}$ bond length is about 0.05 Å longer than the corresponding ones of the doublet and quartet states, in agreement with the singly occupied $\sigma_{xy}*$ orbital in the sextet state, which has antibonding character across the Fe$-$N$_{por}$ bonds. The OOH moiety in all optimized Cpd 0 species bends toward the α-*meso* position of the porphyrin ring. The bond angles ∠FeOO of the FeOOH moiety are in a range of 114.98° to 117.17° for the doublet states of the three studied snapshots (see the SI), which are just a little bit larger than the value (112.5°) recorded for the crystal structure of the oxy HmuO.[9b] These calculated values are close to the corresponding value of the QM/MM optimized Cpd 0 species in HRP (113.5°),[39] but are smaller than the corresponding experimental values of oxy species of some other heme-containing enzymes like myoglobin (122°)[40] and cytochrome P450 (142°, 133°).[41] So the optimized geometries indicate that like the oxy species (PorFe[III]OO⁻), Cpd 0 (PorFe[III]OOH) of HO keeps an acutely bent O$-$O moiety as that in the oxy form. Except for the above-mentioned geometrical features, in all the Cpd 0 species shown in Table 2, there are two additional important features. One is a relatively strong hydrogen bond between the water cluster in the distal pocket and the distal oxygen of the FeOOH moiety (range of the bond distance from 1.742 to 1.841 Å), the other is a hydrogen bond between the distal OH group and one of the nitrogen atoms of the porphyrin ring (range of bond length from 1.969 to 2.120 Å, see the SI document).[42]

3.2.2. Concerted O$-$O Bond Breaking and O$_{distal}$$-C_{α-meso}$ Bond Formation from Cpd 0. Since it was proposed that a concerted O$-$O bond breaking and O$_{distal}$$-C_{α-meso}$ bond formation might account for the mechanism of the heme

(38) (a) Rivera, M.; Caignan, G. A.; Astashkin, A. V.; Raitsimring, A. M.; Shokhireva, T.; Walker, F. A. *J. Am. Chem. Soc.* **2002**, *124*, 6077. (b) Caignan, G. A.; Deshmukh, R.; Zeng, Y.; Wilks, A.; Bunce, R. A.; Rivera, M. *J. Am. Chem. Soc.* **2003**, *125*, 11842. (c) Rivera, M.; Zeng, Y. *J. Inorg. Biochem.* **2005**, *99*, 337. Notice that the labels of orbitals $d_{x^2-y^2}$ and d_{xy} are exchanged in the above literature sources vis-à-vis the labels in this work.
(39) Derat, E.; Shaik, S. *J. Phys. Chem. B* **2006**, *110*, 10526.
(40) Vojtechovsky, J.; Chu, K.; Berendzen, J.; Sweet, R. M.; Schlichting, I. *Biophys. J.* **1999**, *77*, 2153.
(41) (a) Schlichting, I.; Berendzen, J.; Chu, K.; Stock, A. M.; Maves, S. A.; Benson, D. E.; Sweet, R. M.; Ringe, D.; Petsko, G. A.; Sligar, S. G. *Science* **2000**, *287*, 1615. (b) Nagano, S.; Poulos, T. L. *J. Biol. Chem.* **2005**, *280*, 31659.

Table 2. Key Bond Distance R (in Å) of the Three Spin States of Cpd 0 (PorFe^{III}OOH)[a]

	R (Fe–N$_{ImH}$)			R (Fe–O)			R (O–O)			R_{av} (Fe–N$_{por}$)[b]		
snapshot	^2C_R	^4C_R	^6C_R	^2C_R	^4C_R	^6C_R	^2C_R	^4C_R	^6C_R	^2C_R	^4C_R	^6C_R
0 ps	2.039	2.243	2.211	1.838	2.021	1.988	1.461	1.460	1.448	2.035	2.041	2.092
116 ps	2.048	2.339	2.286	1.828	2.014	1.973	1.463	1.458	1.443	2.033	2.037	2.091
287 ps	2.037	2.257	2.240	1.819	1.993	1.966	1.458	1.453	1.440	2.033	2.039	2.091

[a] The left-hand superscript signifies the spin state of the species. [b] The average value of the four Fe–N$_{por}$ bond distances.
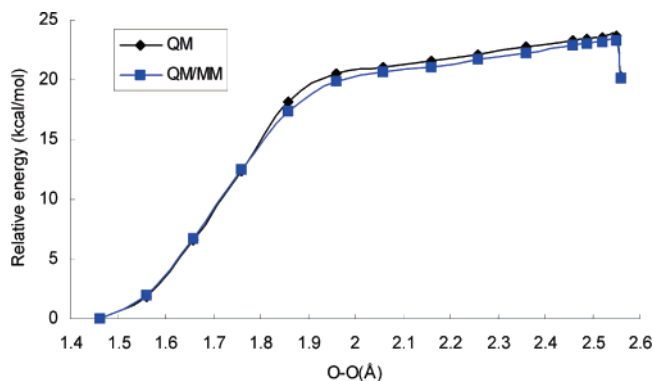

Figure 2. The QM/MM B1 scanned energy profile, for the 0 ps snapshot, along the O–O bond breaking coordinate from ^2C_R on; ^2C_R was taken as the zero of the energy scale.

hydroxylation in HO,[22] here we explored this mechanism within the framework of the QM/MM methodology. For the 0 ps snapshot, our energy profile scan using O$_{distal}$–C$_{\alpha-meso}$ bond as reaction coordinate from ^2C_R (see the SI document Figure S1) leads to an estimated barrier of 63.5 kcal/mol (QM/MM B2//B1). This high value is in agreement with the previous conclusions from QM model calculations (51.6[19a] and 47.4 kcal/mol[23b]). The fact that the QM/MM barrier is so high necessarily means that the concerted process of O–O bond cleavage and O–C$_{meso}$ bond formation from Cpd 0 is not involved in heme degradation by HO.

3.2.3. Stepwise O–O Bond Breaking and O$_{distal}$–C$_{\alpha-meso}$ Bond Formation from Cpd 0. To explore the stepwise mechanism for the heme degradation, we scanned the potential-energy surface (PES) initially by using the O–O bond in Cpd 0 as a reaction coordinate. The obtained profiles are shown in Figures 2, 4, and 5. The key geometries are displayed in Figure 3 and the sequence of structures is depicted in Scheme 4.

As seen from Scheme 4, the O–O bond homolysis generates an intermediate $^2C_{Ia}$ (PorFe^{IV}O[·OH]) in which the OH radical is bound to the water cluster and to a heme nitrogen. Subsequently, there is a conformational rearrangement of the OH radical, whereby the departing OH moiety flips and forms a hydrogen bond between the proximal oxygen of the PorFeO moiety, in $^2C_{Ib}$, which then leads to a *meso*-hydroxylated product, ^2P. The corresponding energy profile of this process is shown in Figures 2 and 4.

Figure 2 reveals that as soon as the O–O bond distance exceeds 2.55 Å, the energy drops somewhat abruptly. This drop was ascertained to result from the conformational change of the flipping of the OH radical upon passage from $^2C_{Ia}$ to $^2C_{Ib}$.

(42) We note that here, in all snapshots, the distal OH group of the OOH moiety adopts a tilted conformation. For the 0 ps and 116 ps snapshots, we also obtained doublet Cpd 0 conformations with an upright orientation of the distal OH, with energies being 0.7 and 3.9 kcal/mol (B2//B1) higher than that of Cpd 0 with the OH tilted. For the 287 ps snapshot, the distal OH upright conformation is not a minimum and it spontaneously relaxed to the distal OH tilted conformation during geometry optimization.
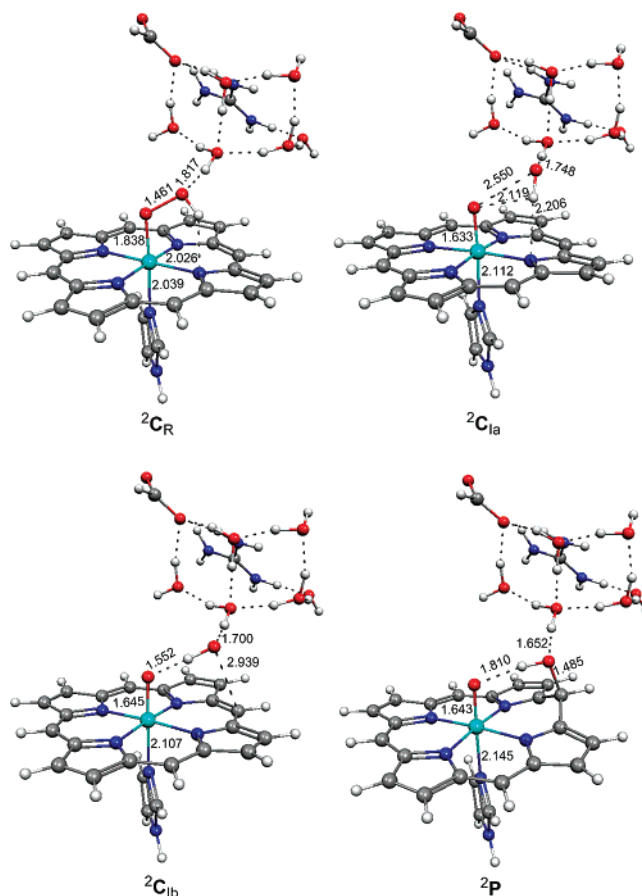
Figure 3. The key geometric parameters during the O–O bond breaking and the O$_{distal}$–C$_{\alpha-meso}$ bond formation from Cpd 0 for the 0 ps snapshot. $^2C_{Ia}$ and $^2C_{Ib}$ are the QM/MM optimized structures before and after the energy "drop" and corresponding to the O–O distances of 2.55 Å ($^2C_{Ia}$) and 2.56 Å ($^2C_{Ib}$). Note the flip of the departing OH group in $^2C_{Ib}$.

This conformational change can be clearly seen in Figure 3 through the structural changes that occur from a geometry just before ($^2C_{Ia}$) to a geometry just after the "drop" ($^2C_{Ib}$). From Figure 3 one can further see that along with the O–O cleavage process, the Fe–O bond length decreases a bit while Fe–N$_{ImH}$ increases. The hydrogen bond between distal OH moiety and the water cluster in the distal pocket is strengthened during the O–O cleavage process.

Since the sudden "drop" in energy can be an artifact of the one-dimensional O–O scan, we further performed a QM/MM two-dimensional scan, in which we employed the breaking O–O bond and the forming O–H hydrogen bond as two scanning coordinates. The result is shown in Figure 4. One can see that on this two-dimensional PES, the transition from Cpd 0 (PorFe^{III}-OOH) to PorFe^{IV}O[·OH] (Cpd II plus OH radical) happens through a "shoulder" region of the PES rather than a well-defined transition state. The single-point calculation at the QM/MM B2 level on the basis of one point of the shoulder region
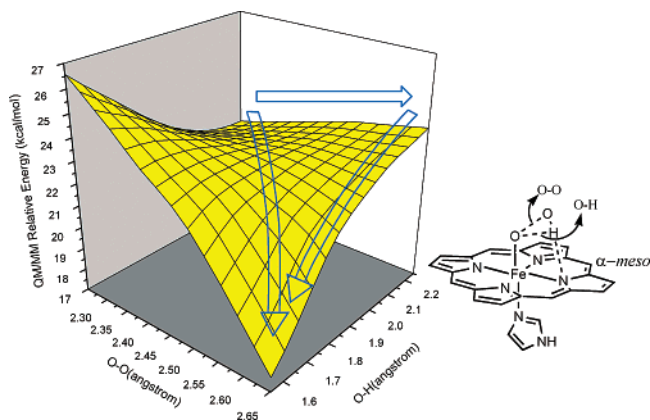
Figure 4. A QM/MM B1 two-dimensional energy scan along the O—O bond-breaking and the H—O hydrogen bond-formation coordinates, for the 0 ps snapshot. ^2C_R was taken as zero of the energy scale. The direction of the "drop" in the one-dimensional scan of Figure 2 is along the two-step head-to-tail arrows, while the diagonal arrow gives the possible minimum energy path.
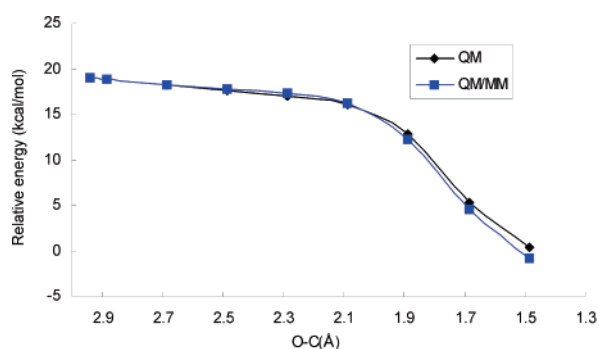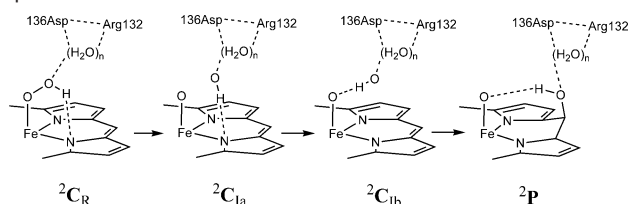

Figure 5. QM/MM B1 energy profile along the forming O—$C_{\alpha-meso}$ bond starting from $^2C_{Ib}$, for the 0 ps snapshot. ^2C_R defines the zero of the energy scale.

Scheme 4. Summary of the Hydroxylation of Heme in HO from Cpd 0

from the two-dimensional scan gives an estimate of the activation energy as 20.00 kcal/mol, while relative to $^2C_{Ia}$, on the one-dimensional scan, this barrier is 20.02 kcal/mol at the same level. As such, the barrier obtained from the highest energy point of the one-dimensional scan provides a good estimate of the activation energy of the O—O cleavage process from Cpd 0.

The QM/MM calculations further demonstrated that the so-produced PorFe^{IV}O[·OH] species after O—O bond homolysis is not a real minimum. The respective energy profile obtained from a scan of PorFe^{IV}O[·OH] along the HO—$C_{\alpha-meso}$ coordinate is shown in Figure 5. From this figure one can clearly see that the OH radical collapses on the α-meso position in a barrier free fashion, to make an O—C bond and produce the hydroxylation product ^2P. So the O—O cleavage followed by the OH radical attack on the α-meso position is *an effectively concerted process*, albeit a nonsynchronous one. Thus, because of the absence of a barrier, for the O—C bond, making the OH radical

Table 3. QM/MM B2 Spin Distribution for Species during the Heme Degradation Process from Cpd 0 of the 0 ps Snapshot[a]

	Fe	O proximal	OH distal	ImH (His20)	porphyrin
^2C_R	0.95	0.10	0.00	−0.01	−0.05
$^2C_{Ia}$	1.37	0.59	−0.84	0.00	−0.13
$^2C_{Ib}$	1.42	0.64	−0.86	0.00	−0.21
^2P	1.42	0.67	−0.02	−0.01	−1.06
^4C_R	2.76	0.20	0.03	0.08	−0.08
^6C_R	4.21	0.25	0.04	0.09	0.41

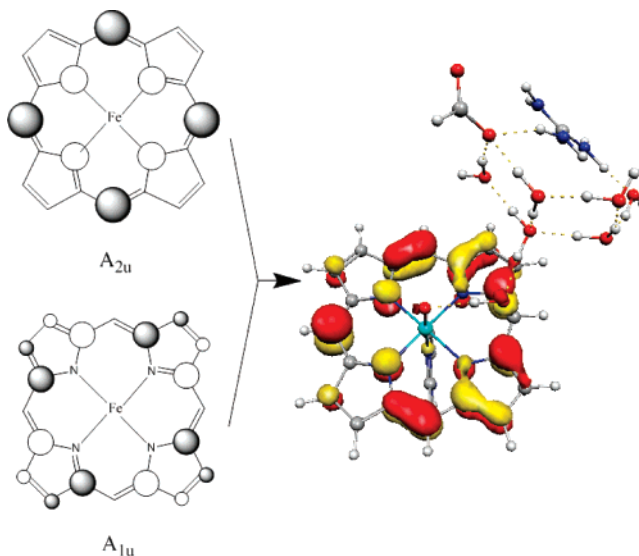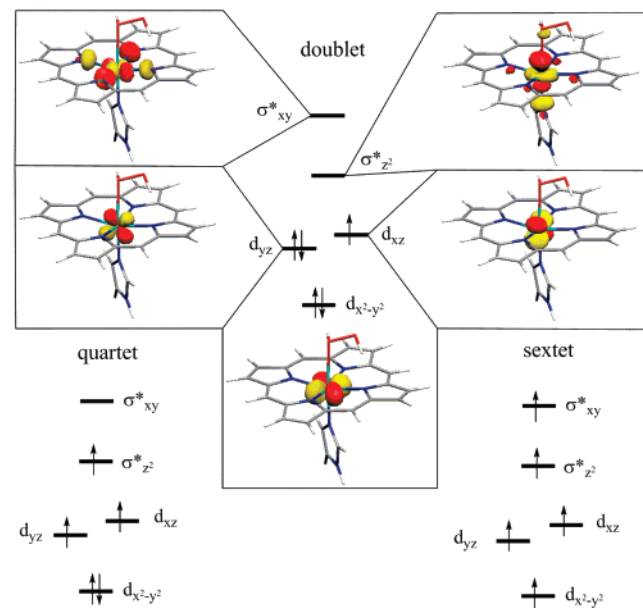[a] The left-hand superscript signifies the spin state of the species.

Figure 6. The singly occupied Kohn—Sham orbital of the porphyrin ring of ^2P.

could only have an ultrashort lifetime, and once it is produced it will attack the α-meso position instantaneously.

In Table 3 we collect the spin distribution of the species in the above-described effectively concerted heme degradation from Cpd 0 for the 0 ps snapshot. The spin distributions of $^2C_{Ia}$, $^2C_{Ib}$, and ^2P show they all are triradicaloid species and have a typical ferryl Fe^{IV}=O unit, in which the two Fe=O π* orbitals are singly occupied. The two Fe=O π* electrons are ferromagnetically coupled to a triplet, and this triplet unit is antiferromagnetically coupled with the third unpaired electron to form doublet states. The third unpaired electron resides in an orbital of the departing OH radical, in $^2C_{Ia}$ and $^2C_{Ib}$, while in ^2P the OH-radical attack to form the O—C_{meso} bond results in the transfer of the radical to the porphyrin ring. Orbital analysis for ^2P shown in Figure 6 indicates the singly occupied π-type orbital of the porphyrin ring is a mixture of the A$_{2u}$- and A$_{1u}$-type orbitals of the well-established porphyrin iron-oxo species, but the component of the α-meso carbon p-orbital is disconnected because this orbital is being used to form the O—$C_{\alpha-meso}$ bond in the hydroxylation product ^2P. As a result of the α-meso carbon hydroxylation in ^2P, the conjugation of the porphyrin ring is broken and the extension range of the π-type orbital is reduced, hence the orbital increases in energy easily and loses its electron in subsequent steps. This propensity will be discussed later in the study of the surrogate reaction.

Since the calculation for the 0 ps snapshot has indicated that O—O cleavage process is the rate-determining step and the subsequent OH attack on the α-meso carbon is barrierless, we

Scheme 5. Orbital Occupancies of FeHOOH Species for the Doublet, Quartet, and Sextet States

Table 4. QM(UB3LYP)/MM(CHARMM) Relative Energies (kcal/mol) for Three Spin States of the FeHOOH Species, with B1 and B2[a]

spin state	singly occupied orbitals	snapshot 0 ps		snapshot 116 ps		snapshot 287 ps	
		B1	B2	B1	B2	B1	B2
^4C_RH	π_{yz}^*	0.00	0.00	0.00	0.00	0.00	0.00
^2C_RH	$\pi_{yz}^*d_{xz}\sigma_{z^2}^*$	3.68	2.77	2.94	5.06	2.57	4.70
^6C_RH	$\sigma_{xy}^*d_{x^2-y^2}\pi_{yz}^*d_{xz}\sigma_{z^2}^*$	8.95	4.66	6.68	5.24	6.54	5.26

[a] The left-hand superscript signifies the spin state of the species.

only explored the O−O cleavage process for the other two snapshots, 116 and 287 ps. Our calculations (see the SI document Figures S3 and S5) gave O−O bond cleavage barriers of 17.5 and 19.6 kcal/mol at the QM/MM B2 level, respectively, slightly smaller but close to the barrier in the 0 ps snapshot. Interestingly, in cytochrome P450 a similar mechanism starts with O−O bond homolysis but leads to the formation of Cpd I (Por$^{+\bullet}$Fe^{IV}=O), with a smaller activation barrier, ranging between 13 and 14 kcal/mol.[43] The major difference between the two mechanisms is that in P450 the cysteinate ligand raises the A$_{2u}$ orbital in energy and causes thereby a concomitant electron transfer from the heme to the departing OH radical that undergoes, in turn, a spontaneous protonation and leads to the formation of Cpd I. This is the famous "push effect" of the cysteinate ligand,[2] which is absent in HO.

3.2.4. Iron Hydrogen Peroxide Complex (Fe^{III}HOOH). Since, experimentally, H$_2$O$_2$ can be used to promote HO-catalyzed degradation of heme, it is indeed necessary to explore the mechanism of this surrogate reaction. First, we studied the PorFe^{III}HOOH complex, labeled C_RH. The orbital occupations for three spin states of C_RH are shown in Scheme 5. Comparing the doublet state for PorFe^{III}HOOH to Cpd 0 (PorFe^{III}OOH) in Scheme 3, one can see that the singly occupied orbitals are different and involve two orthogonal iron d orbitals d_{yz} and d_{xz}, respectively, reflecting the weakened Fe−O bonding.

In Table 4 we summarized the calculated energies for the three spin states of PorFe^{III}HOOH. For all the studied snapshots, the spin-state ordering from low to high energy is quartet, doublet, and sextet state. The ground state is the quartet state and the second lowest state in energy is the doublet state, with the sextet state being slightly higher in energy.

In Table 5 we collected the key geometric parameters for the three spin states of PorFe^{III}HOOH in the studied snapshots. One can see that the Fe−O bond distances of the PorFe^{III}HOOH species are quite longer than those of the corresponding Cpd 0,

(43) Zheng, J.; Wang, D.; Thiel, W.; Shaik, S. *J. Am. Chem. Soc.* **2006**, *128*, 13204.

which indicates that Fe−O bond is weaker in PorFe^{III}HOOH than in Cpd 0. For the 0 ps snapshot, in the quartet state, the H$_2$O$_2$ molecule forms hydrogen bonding with the water cluster, and has completely dissociated from the Fe center, having extremely long Fe−O distance (3.442 Å). As such, for ^4C_RH it is possible to explore the potential deprotonation of H$_2$O$_2$ before it coordinates to the iron center to form Cpd 0. However, our QM/MM geometry optimization for the protonated Asp136 plus $^-$OOH anion system collapsed back to the state of deprotonated Asp136 plus HOOH. Although we first did partial optimization by constraining the proton released from HOOH and kept it in the Asp136/water cluster, after removing the constraint, the proton shuttled back to $^-$OOH to produce HOOH. The optimized geometry with this constraint is higher in energy relative to ^4C_RH (by about 18.5 kcal/mol at the QM/MM B1 level). Taken together, these results imply that the deprotonation of the H$_2$O$_2$ before its coordination with iron is thermodynamically disfavored. There remains then, the possibility that HOOH gets deprotonated after its coordination with iron, for example, from ^2C_RH. To assess the possibility of this process, we calculated the energies of the system before and after this deprotonation happens. We found that the energy of the doublet state for protonated Asp136 plus Cpd 0 system, which is the ground state after deprotonation, is about 15.0 kcal/mol higher than ^2C_RH at the QM/MM B2 level. This means that the water cluster/Asp136(-) is stable as an anionic entity, due to the multiple hydrogen bonds (H-bonds) that link the water to the aspartate anion and the arginine cation, and disfavors the deprotonation of ^2C_RH since this leads to weakening of the H-bonding network. Therefore it can be expected that the PorFe^{III}HOOH complex will remain intact in the HO active site.

In the optimized structures of the quartet states of the other two snapshots, hydrogen peroxide still coordinates with iron, although in these quartet state structures, the Fe−O bond distances are much longer than those in the doublet states due to the singly occupied $\sigma_{z^2}^*$ orbital in the quartet states. So generally for PorFe^{III}HOOH, the Fe−O bond in the doublet state is stronger than those in the quartet state and in the sextet state. Our calculations also reveal that the optimized geometry for the doublet state is a local minimum of the ground state because at the geometry of this minimum, the quartet state is 7.41, 4.19, and 3.58 kcal/mol higher than the doublet state for the 0, 116, and 287 ps snapshots, respectively. So although the double state of PorFe^{III}HOOH is not the global minimum of the ground state, it is possible that the doublet state is metastable state at the geometrical region with short Fe−O bond like that in ^2C_RH.

Interestingly, the optimized Fe−O bond in the quartet state, ^4C_RH, in Table 5 is shortened significantly on going from the 0 ps snapshot to the 116 and 287 ps snapshots, while the energy

Table 5. Key Bond Distance R (in Å) of the Three Spin States of PorFe^{III}HOOH Species[a]

	R (Fe–N$_{ImH}$)			R (Fe–O)			R(O–O)			R_{av} (Fe–N$_{por}$)[b]		
snapshot	^2C_R	^4C_R	^6C_R	^2C_R	^4C_R	^6C_R	^2C_R	^4C_R	^6C_R	^2C_R	^4C_R	^6C_R
0 ps	1.912	2.077	2.041	2.187	3.442	2.588	1.457	1.453	1.453	2.025	2.022	2.081
116 ps	1.926	2.123	2.084	2.209	2.516	2.558	1.457	1.455	1.456	2.017	2.018	2.070
287 ps	1.924	2.113	2.074	2.262	2.620	2.653	1.451	1.449	1.449	2.019	2.019	2.070

[a] The left-hand superscript signifies the spin state of the species. [b] The average value of the four Fe–N$_{por}$ bond distances.
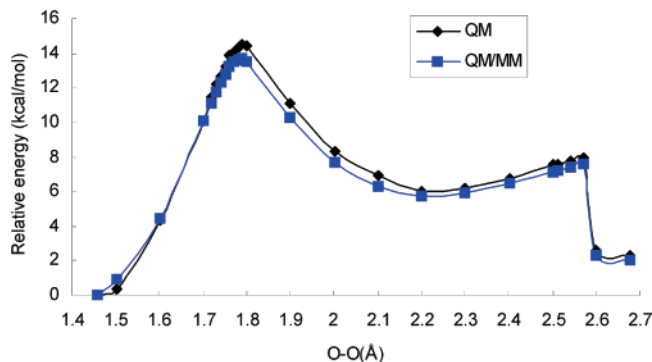

Figure 7. The QM/MM B1 scanned energy profile along the breaking O–O bond from ^2C_RH, for the 0 ps snapshot. ^2C_RH was taken as zero of the energy scale.

is rather flat. It is conceivable that there are a few minima for this complex, some with long Fe–O bond and others with a shorter bond, and their energies are given as a balance between the strength of the Fe–O bond vis-à-vis the stabilization of the H$_2$O$_2$ by hydrogen bonding near the water cluster. Analogous findings were reported for complexes in P450.[44]

3.2.5. Concerted O–O Bond Breaking and O$_{distal}$–C$_{\alpha-meso}$ Bond Formation from PorFe^{III}HOOH. Similar to the Cpd 0 case, here we also explored the possibility of the concerted O–O bond cleavage and O–C$_{meso}$ bond formation as a potential heme degradation mechanism. For the 0 ps snapshot, we used the O–C$_{meso}$ distance as reaction coordinate to scan the energy profile from ^2C_RH. However, during this scan, the Fe–O bond breaks and the coordination of H$_2$O$_2$ with iron is totally lost. The reason for this behavior, as mentioned in section 3.2.4. is that the Fe–O bond in PorFe^{III}HOOH is weaker than that in Cpd 0. Our calculations thus do not support the concerted mechanism of the heme degradation process from PorFe^{III}-HOOH as well.

3.2.6. Stepwise O–O Bond Breaking and O$_{distal}$–C$_{\alpha-meso}$ Bond Formation from PorFe^{III}HOOH. Let us turn to the stepwise mechanism in Figures 7–9. The overall reaction sequence is schematically shown in Scheme 6.

Inspection of Scheme 6 shows that O–O bond homolysis of ^2C_RH proceeds via a transition state, $^2TS_{OO}H$ leading to an intermediate Por$^{•+}$Fe^{III}OH[•OH] labeled $^2C_{Ia}H$, in which the OH radical is bound to the heme and to the water cluster by hydrogen bonds. Subsequently the OH radical flips and switches hydrogen bonding to the FeOH moiety in $^2C_{Ib}H$, and subsequently hydroxylates the heme to form ^2PH.

Figure 7 scans the energy profile along the breaking O–O bond from ^2C_RH in the 0 ps snapshot. Thus, after the O–O cleavage, the intermediate $^2C_{Ia}H$ (Por$^{•+}$Fe^{III}OH[•OH]) is formed with a barrier of 11.02 kcal/mol at the QM/MM B2 level. Then

(44) (a) Lin, H.; Schoneboom, J. C.; Cohen, S.; Shaik, S.; Thiel, W. *J. Phys. Chem. B* **2004**, *108*, 10083. (b) Schoneboom, J. C.; Thiel, W. *J. Phys. Chem. B* **2004**, *108*, 7468.

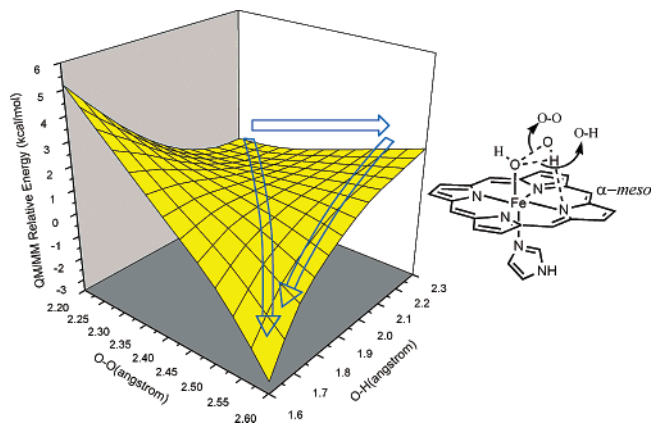**Figure 8.** A QM/MM B1 two-dimensional scan from $^2C_{Ia}H$ along the O–O bond breaking and the forming H–O hydrogen bond, for the 0 ps snapshot. $^2C_{Ia}H$ was taken as zero of the energy scale. The direction of the "drop" in the one-dimensional scan of Figure 7 is along the two-step head-to-tail arrows, while the diagonal arrow gives the possible minimum energy path.

$^2C_{Ia}H$ evolves to $^2C_{Ib}H$ with a barrier of 1.88 kcal/mol at the QM/MM B2 level. Figure 9 shows that the transformation between the two intermediates involves indeed the flipping of the OH radical. From the 2-D scan plotted in Figure 8 along O–O bond breaking and O–H H-bond formation, the estimated barrier for the conformation change from $^2C_{Ia}H$ to $^2C_{Ib}H$ decreases to 1.33 kcal/mol at the QM/MM B2 level. The Por$^{•+}$-Fe^{III}OH[•OH] species in $^2C_{Ib}H$, is 3.57 kcal/mol lower in energy than ^2C_RH at the QM/MM B2 level and is hence quite stable. This result is quite different from the QM model calculation done by the same group[19a] (there the Por$^{•+}$Fe^{III}OH[•OH] intermediate cluster is 13.3 kcal/mol higher than PorFe^{III}HOOH), which indicates the protein environment stabilizes the OH radical formation very much. Figure 8 shows that in a two-dimensional scan there is no sudden drop in energy as portrayed in Figure 7, but there is a smooth energy path along the two coordinates, with a preorganization of the H-bonding followed by O–O breakage.

Through the above conformational changes of the H-bonding network (consult also Figure 9), the OH radical $^2C_{Ib}H$ is suitably oriented to attack the α-*meso* position of the porphyrin. Figure 10 displays the energy profile scan from $^2C_{Ib}H$ to the α-*meso* carbon hydroxylation product ^2PH, using (H)O–C$_{\alpha-meso}$ as reaction coordinate. We can see that after a flat region of about 0.5 Å, the energy begins to decrease down to ^2PH. Thus, after the conformational change, the process of the OH radical attack on α-*meso* carbon from $^2C_{Ib}H$ is barrierless.

There exists however another potential pathway from $^2C_{Ia}H$; this is the formation of Cpd I (Por$^{+•}$Fe^{IV}=O) plus water through hydrogen abstraction from proximal oxygen atom by OH radical. Our scan of this process indicates (see Figure S2 in the Supporting Information) a barrier of 3.5 kcal/mol at the QM/MM B2 level. Although this barrier is larger than the one estimated (1.3 kcal/mol) for the conformation change from $^2C_{Ia}H$ to $^2C_{Ib}H$, the barriers are close enough to suggest a competition
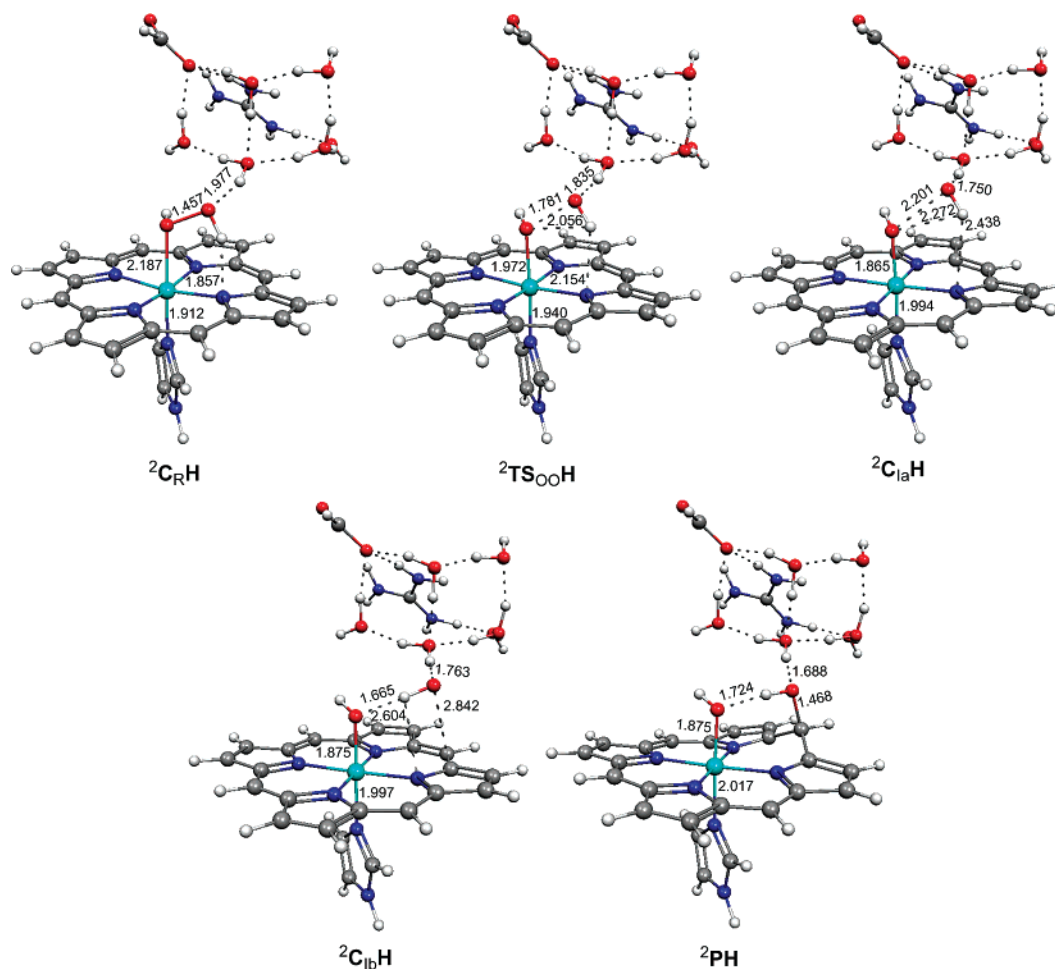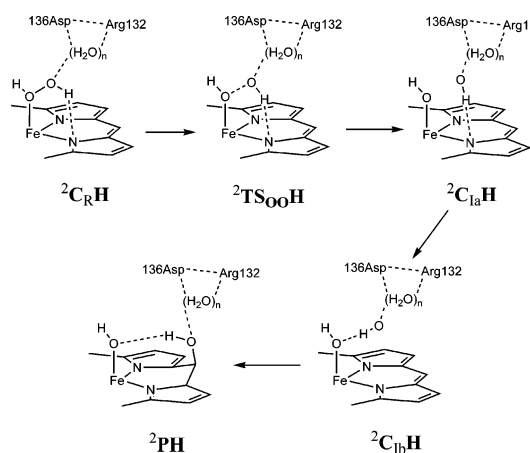
Figure 9. The key structures in the process of stepwise O—O bond breaking and O_{distal}—$C_{\alpha-meso}$ bond formation from PorFe^{III}HOOH for the 0 ps snapshot.

Scheme 6. Summary of the Hydroxylation of Heme in HO from PorFe^{III}HOOH

Figure 10. The scan energy profile along the forming O—$C_{\alpha-meso}$ bond from $^2C_{Ib}H$ at the QM/MM B1 level for the 0 ps snapshot. ^2C_RH was taken as the zero of the energy scale.

between these two processes, especially when perturbation of the distal pocket by the mutation of some residues is introduced. This competition will limit the efficiency of the surrogate process of H_2O_2 to hydroxylate the *meso* position.

3.2.6.1. The Impact of the Water Cluster and the Surrounding Protein. The crucial roles of the water cluster and interplay with the surrounding protein are apparent from the QM/MM optimized geometries of the critical species in Figure 9 and the spin density development in Table 6. Thus, the protein environment promotes the electron transfer from porphyrin to
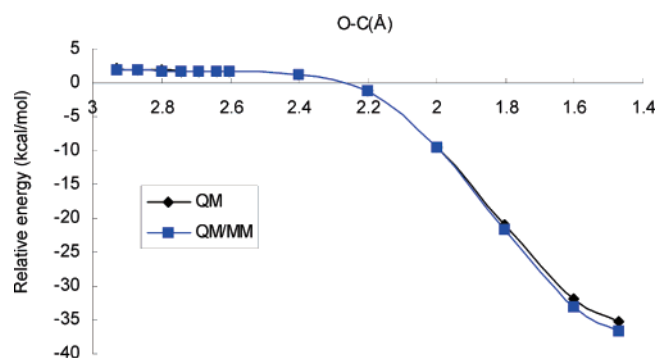
Fe—O unit at the early stage of the O—O cleavage, and thereby assists the cleavage (consult the spin development on the porphyrin in Table 6). Furthermore, one can see that in $^2TS_{OO}H$ (Figure 9), the O—O bond distance is only 1.781 Å, namely, much shorter than the distance obtained (2.096 Å) in the previous QM model calculation.[19a] It is further seen that the hydrogen bond between the water cluster and the distal O atom of the PorFeHOOH species persists all the way to ^2PH, and its strength keeps increasing, as indicated by the decreasing hydrogen bond distance. This may be one of the reasons for the extra stabilization of the OH radical species $^2C_{Ia}H$ and $^2C_{Ib}H$, compared with the QM-only investigation.[19] During the whole reaction process, the water cluster in the distal pocket

Table 6. QM/MM B2 spin Distribution for Structures in the Heme Degradation from the PorFe^{III}HOOH Species of the 0 ps Snapshot[a]

species	Fe	OH proximal	OH distal	ImH (His20)	porphyrin
^2C_RH	1.04	−0.01	0.00	0.00	−0.03
$^2TS_{OO}H$	0.91	−0.09	−0.35	0.02	0.51
$^2C_{Ia}H$	0.94	−0.18	−0.73	0.02	0.96
$^2C_{Ib}H$	0.97	0.04	−0.89	0.02	0.85
^2PH	1.00	0.03	0.00	0.01	−0.05
^4C_RH	2.80	0.00	0.00	0.14	0.05
^6C_RH	4.17	0.02	0.00	0.15	0.66

[a] The left-hand superscript signifies the spin state of the species.

keeps its shape and appears to be quite stable. The Fe−O bond length increases by about 0.2 Å from ^2C_RH to $^2TS_{OO}H$, and then decreases to about 1.87 Å in $^2C_{Ia}H$, $^2C_{Ib}H$ and ^2PH.

3.2.6.2. Electronic Differences between PorFe^{III}HOOH and PorFe^{III}OOH Degradations and Comparison to NOS. In Table 6 we collected the spin population of the species in the stepwise heme degradation from ^2C_RH. One can see that there exists a significant difference between this Table for the PorFe^{III}-HOOH case and Table 3 for the Cpd 0 (PorFe^{III}OOH) case. Along the reaction path, from $^2TS_{OO}H$ through $^2C_{Ia}H$ to $^2C_{Ib}H$, all the three species, $^2TS_{OO}H$, $^2C_{Ia}H$, and $^2C_{Ib}H$ have substantial spin distribution on the porphyrin ring. Further analysis indicates the partial occupied porphyrin orbital is mainly an A$_{2u}$-type π orbital of the porphyrin ring (tiny mixing with the A$_{1u}$-type π orbital). However, in the reactant ^2C_RH the A$_{2u}$-type π orbital of the porphyrin ring is doubly occupied. This means during the reaction process, A$_{2u}$-type π orbital of the porphyrin ring loses one electron. This electron is indeed transferred to the ferryl Fe^{IV}OH unit to produce a ferric iron. It is interesting to notice that this result is similar to the recent QM/MM finding in nitric oxide synthase (NOS uses cysteine as proximal ligand rather than histidine as in HO), in which the homolytic O−O cleavage from the PorFe^{III}HOOH species was found to be accompanied by one electron transfer from the porphyrin ring to the ferryl Fe^{IV}=O unit (in the case of NOS, this O−O cleavage leads however to Cpd I formation).[45] The unusually short distance of the breaking O−O bond in $^2TS_{OO}H$ (Figure 9) appeared also in the mechanism of NOS and is also likely to be related to the formation in both of the porphyrin hole electronic configurations. However, one noticeable difference between HO and NOS is that in NOS, the Cpd I formation following O−O cleavage was calculated to be barrierless, while, here in HO, a conformational change of the OH radical followed by attack of the porphyrin ring is preferred over the Cpd I formation.

In the hydroxylation product ^2PH of PorFe^{III}HOOH, and in contrast to ^2P in the case of Cpd 0, there is no spin distribution on the porphyrin ring. The reason for this difference is that the porphyrin π-type orbital, which is singly occupied in ^2P, has provided its electron to the ferryl Fe^{IV}OH unit to produce ferric iron Fe^{III}−OH in ^2PH, and hence the porphyrin π-type orbital becomes vacant in ^2PH, and the respective porphyrin ring is a closed-shell cation. So along the entire stepwise heme degradation reaction path from ^2C_RH, the iron is in the ferric state rather than in the ferryl state. The result here also indicates if the hydroxylation product ^2P from Cpd 0 gets protonated in the

proximal oxygen position during heme hydroxylation, something which is shown below to be highly profitable, then the ferryl unit will be reduced to a ferric state and porphyrin will appear as closed-shell cation.

Since the result for the 0 ps snapshot has indicated that the O−O cleavage process producing an OH radical is the rate-determining step from ^2C_RH to ^2PH, and the subsequent OH radical attack on α-*meso* position of the porphyrin ring is barrierless (following a small barrier for the conformational rearrangement of $^2C_{Ia}H$ to $^2C_{Ib}H$ see Figure 8), for the 116 and 287 ps snapshots, we only explored the O−O cleavage. Here we summarize the most important results (for more detailed results see the SI document, Figures S4 and S6). The O−O cleavage barriers for the 116 and 287 ps snapshots, were calculated to be 13.45 and 12.92 kcal/mol, respectively. Although the protein environment and the water cluster in the distal pocket changes a lot from the 0 ps snapshot to the 116 ps and the 287 ps snapshots, the O−O bond in the $TS_{OO}H$ transition state remains short, ca. 1.80 Å. In these two snapshots too, homolytically cleaved PorFe^{IV}OH[·OH] intermediate is still stable being −0.66 and 0.75 kcal/mol relative to ^2C_RH (QM/MM B2//B1). This highlights a possible intrinsic propensity of HO to stabilize the OH radical generated from ^2C_RH.

3.2.7. The Possible Timing of Proximal Oxygen Protonation During the Native Route. Since, as discussed above, the intermediates in the surrogate route are highly stabilized, compared with the native route, it is arguable that during the latter route that starts with Cpd 0, we should observe an increased propensity for protonating the proximal oxygen. Indeed, our QM/MM calculations (see Table S4 in the SI) show that if the Asp136 is protonated in the onset of the native route, the product ^2P becomes 50.2 kcal/mol (QM/MM B2) higher in energy than the product where the proximal oxygen is protonated, and which is identical to ^2PH. This result strongly indicates that along the native hydroxylation route of the heme, the basicity of the forming iron-oxo species (PorFe^{IV}=O; i.e., Cpd II) is large enough to abstract a proton from the protonated Asp136/water cluster.[46] While the mechanism for the proximal protonation is not clear, in view of the chasm between the cluster and the proximal oxygen of the heme, still the result in itself is consistent with the conclusion from proton inventory analysis that the heme hydroxylation by Cpd 0 is attended by proton delivery.[22]

4. Discussion

4.1. The Nature of the Heme Degradation Mechanism in the Native Route. By exploring the heme degradation from Cpd 0 using the QM/MM method, we have shown that the mechanism, in which O−O cleavage and O−C$_{\alpha-meso}$ bond formation proceed sequentially, is much lower in energy than the fully concerted/synchronous mechanism. This result is consistent with the previous QM model calculations.[19,23] However, one important difference between the results here and the previous QM model calculation is that the second step of the O−C$_{\alpha-meso}$ bond formation is found to be barrierless here rather than having a small barrier as in the previous gas-phase QM calculation. This means that after considering the effect of the protein environment, the OH radical produced in the initial O−O cleavage does not reside in a stable minimum any more

(45) Cho, K.-B.; Derat, E.; Shaik, S. *J. Am. Chem. Soc.* **2007**, *129*, 3182.

(46) Green, M. T.; Dawson, J. H.; Gray, H. B. *Science* **2004**, *304*, 1653.

and will spontaneously attack the α-*meso* carbon atom. As such, the lifetime of the hydroxyl radical produced in HO is likely to be extremely short and the mechanism is effectively concerted albeit nonsynchronous. An effectively concerted mechanism is in accord with mechanistic conclusions from recent isotope effect experiments.[22] The ultrashort lifetime expected for the intermediate, may explain why OH radical, a highly toxic species in the biological systems, can still be produced in HO. Its formation is merely formal.

4.2. Functions of the Water Cluster in the Distal Pocket. In all the three studied snapshots, we found that the water cluster in the distal pocket controls the produced OH radical by a strong hydrogen bond. As shown in Figure 3 and Figure 9, for heme degradations both from PorFe^{III}OOH (Cpd 0) and from PorFe^{III}-HOOH, this hydrogen bond is retained and increases its strength during the whole reaction process from the reactant ^2C_R and ^2C_RH to the product ^2P and ^2PH. No doubt, this distal water stabilizes the OH radical on the one hand, and on the other, it controls the movement of the OH radical and ensures its exclusive orientation toward an eventual attack on the α-*meso* position of the porphyrin ring. The water cluster acts also as a protecting and insulating layer between OH radical and the distal residues of the protein; it thereby avoids also the deleterious effects of OH radicals. Thus, the distal water cluster has an important strategic function in HO enzymes.

4.3. The H$_2$O$_2$ Surrogate Reaction. On the basis of our results here for the PorFe^{III}HOOH active species, we propose that the active species is different than the one in the native process. Despite the belief that this surrogate reaction also proceeds through a Cpd 0 intermediate, in fact, there are no acidic or basic residues near the iron coordinate center in HO, which can deprotonate the proximal OH group of PorFe^{III}HOOH and thereby form Cpd 0. This is demonstrated by the endothermic deprotonation processes calculated above by QM/MM.

The QM/MM calculations show that PorFe^{III}HOOH follows a similar formally stepwise reaction path like that from Cpd 0. First, O—O cleavage takes place to produce a bound OH radical. Then, following a small barrier (1.3 kcal/mol), the conformationally relaxed OH radical attacks the α-*meso* position of the porphyrin ring in a barrier-free process and forms the hydroxy-heme product. The respective barrier on the doublet surface is 11.0 kcal/mol for the 0 ps snapshot. After considering the energy difference between the quartet ground state and the doublet state, the activation energy is still only 13.8 kcal/mol. This is even lower than the calculated activation energy from Cpd 0 species. However, experimentally, for HmuO the H$_2$O$_2$ surrogate reaction was found to be less efficient than the native reaction via Cpd 0. One possible reason for that is that in the surrogate reaction, because of a small barrier for conformational relaxation of the radical, heme-hydroxylation competes with Cpd I formation, while in the native reaction of Cpd 0 there is no competition to heme-hydroxylation. Another reason is the instability of the PorFe^{III}HOOH complex, as revealed in our calculations for the 0 ps snapshot. Thus, H$_2$O$_2$ could not form a stable coordination complex with iron in the quartet ground state. This result, in association with the high-spin ground state found for six-coordinated ferric heme iron in HO with sixth ligand being water,[14b,47] implies that the coordination of H$_2$O$_2$ to iron in HmuO may be an inefficient process, thus adversely affecting the heme-hydroxylation reactivity.

Scheme 7. Proposed Origins of the Observed SKIE in Heme-Hydroxylation[22]
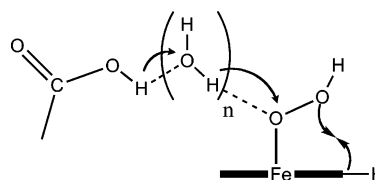
4.4. The Observation of Solvent Kinetic Isotope Effect during the Native Route. Experimentally, significant solvent kinetic isotope effect (SKIE) was observed in the first heme degradation step of hydroxylation of the α-*meso* position of the porphyrin ring. To explain this observation, a proton transfer (to proximal oxygen) was surmised to assist the O—O cleavage and the distal oxygen attack on the α-*meso* carbon of the porphyrin ring from Cpd 0 was proposed,[22] as shown in Scheme 7.

Model QM calculations supported this proposal and reproduced the observed SKIE.[19b] However, the QM/MM calculations based on HO crystal structure here, reveal no structural motif that can form a H-bonding network linked to the proximal oxygen atom and to some acidic residue. This is because in the crystal structure there are two glycine residues (Gly135 and Gly139) near the proximal oxygen atom and they prohibit interaction between the proximal oxygen and the carboxylic group of Asp136 through a relay action of a water cluster in the distal pocket. In fact, the distal water cluster is remarkably robust, and it survived the classical MD simulation. We further did not observe any water H-bond network approaching the proximal oxygen atom in the trajectory. However, there are two facts that bring together experiment and theory: First, the water cluster undergoes reorganization and the H-bonds to the distal OH are changing during the process. Since the water cluster and its H-bonding interactions are tightly knitted, this may well be responsible for the observed SKIE. Second, our QM/MM energetic calculations indicated that the proximal oxygen has a greater propensity to be protonated as the heme hydroxylation process advances. Since the entire process is effectively concerted, it is conceivable that the experimental observation of SKIE[22] is associated with such a proton delivery.

4.5. Comparison between the Native Routes of P450 and HO and Relation to HRP. A central question in heme enzymes concerns the difference between P450 and HO. In both enzymes there is a similar O$_2$ activation mechanism that generates Cpd 0 (PorFe^{III}OOH). However, while HO stops at Cpd 0 and uses it to activate the *meso* position of the porphyrin, P450 continues further to Cpd I (Por$^{+•}$Fe^{IV}=O)^2 and uses it to activate substrates. Theoretical calculations here and elsewhere[43] show that the mechanisms are very similar and yet entirely different. Thus, in both enzymes the O—O bond activation is essentially homolytic. But whereas in HO the departing OH· radical collapses on the *meso* position, in P450 the radical accepts an electron from Cpd II (PorFe^{IV}=O) that in turn becomes Cpd I and, at the same time, gets protonated via the Asp-H$_2$O-Thr

(47) (a) Sun, J.; Wilks, A.; Ortiz de Montellano, P. R.; Loehr, T. M. *Biochemistry* **1993**, *32*, 14151. (b) Takahashi, S.; Wang, J.; Rousseau, D. L.; Ishikawa, K.; Yoshida, T.; Host, J. R.; Ikeda-Saito, M. *J. Biol. Chem.* **1994**, *269*, 1010. (c) Takahashi, S.; Wang, J.; Rousseau, D. L.; Ishikawa, K.; Yoshida, T.; Takeuchi, N.; Ikeda-Saito, M. *Biochemistry* **1994**, *33*, 5531. (d) Hirotsu, S.; Chu, G. C.; Unno, M.; Lee, D. S.; Yoshida, T.; Park, S. Y.; Shiro, Y.; Ikeda-Saito, M. *J. Biol. Chem.* **2004**, *279*, 11937.

channel. The major difference between the two enzymes is the proximal ligand:[48,49] in P450 the cysteinate ligand raises the A_{2u} orbital in energy, while the histidine ligand in HO does not affect the A_{2u} orbital, which remains low. As such, P450 Cpd II is a powerful reductant compared to HO, and therefore P450 Cpd II can transfer an electron to the departing OH· radical and facilitates its protonation. In contrast, in HO the departing OH· radical is not reduced and, being held by the distal water cluster in a strategic position, it collapses onto the *meso* position of the porphyrin.

Another interesting relation is to horseradish peroxidase (HRP), where Cpd 0 undergoes heterolytic cleavage[39] and generates Cpd I. The difference between HO and HRP, which share the same proximal ligand, is in the nature of the protein pocket. In HRP, the pocket contains the His-water-Arg system that is strategically placed and can shuttle protons to and from the heme in the Poulos−Kraut mechanism.[39,50] In HO such a system is absent, and therefore HO minimizes its peroxidase activity and proceeds to activate the heme as described above. Small differences that make bigger differences!

5. Conclusions

The QM/MM calculations in this paper indicate that the HO catalyzed heme degradation starting from either Cpd 0 or PorFe^{III}HOOH proceeds via a mechanism that involves first O−O homolytic cleavage to generate OH radical species followed by HO−C$_{meso}$ bond formation. The second step of the OH radical attack on the α-*meso* position of porphyrin is barrier free, albeit a small barrier exists in the surrogate reaction for the OH conformation orientation. As a result, *the mechanisms are effectively concerted nonsynchronous processes* and the lifetime of the generated OH radical is most likely too short to qualify as such. In both cases, either through Cpd 0 or Fe^{III}-HOOH, the fully concerted mechanism of O−O breaking and O−C$_{meso}$ forming is highly disfavored in energy.

The water cluster in the distal pocket plays a crucial role in controlling the barrier for the O−O cleavage process, and more importantly it is responsible for the observed regiochemistry of hydroxylation. Thus, by tightly holding the hydroxyl radical, *the water cluster fixes an orientation conducive to exclusive attack on the α-meso position of the porphyrin*. Thus, the water cluster is responsible for creating function in OH by converting a very nonselective reaction of a highly reactive species to a regio-specific and highly efficient process of α-*meso* hydroxylation.

The H_2O_2 surrogate reaction in HO is likely to proceed through Fe^{III}HOOH. In HmuO it is less efficient than the native process via Cpd 0 for two reasons: one is the potential competition of Cpd I formation as reported for NOS[45] and another is the instability of the Fe^{III}HOOH complex.

Supporting Information Available: Computational procedures, scan energy profiles, *x,y,z* coordinates, energies, spin and charge population of the various species, and complete refs 27 and 31. This material is available free of charge via the Internet at http://pubs.acs.org.

(48) de Visser, S. P.; Shaik, S.; Sharma, P. K.; Kumar, D.; Thiel, W. *J. Am. Chem. Soc.* **2003**, *125*, 15779.
(49) Ogliaro, F.; de Visser, S. P.; Shaik, S. *J. Inorg. Biochem.* **2002**, *91*, 554.
(50) (a) Poulos, T. L.; Kraut, J. *J. Biol. Chem.* **1980**, *255*, 8199. (b) Derat, E.; Shaik, S.; Rovira, C.; Vidossich, P.; Alfonso-Prieto, M. *J. Am. Chem. Soc.* **2007**, *129*, 6346.

JA076679P